

Reentrant spin reorientation transition and Griffiths-like phase in antiferromagnetic $\text{TbFe}_{0.5}\text{Cr}_{0.5}\text{O}_3$

Bhawana Mali,^{1,*} Harikrishnan S. Nair,² T. W. Heitmann,³ Hariharan Nhalil,^{1,†} Daniel Antonio,⁴ Krzysztof Gofryk,⁴ Shalika Ram Bhandari,^{5,6} Madhav Prasad Ghimire,^{5,6} and Suja Elizabeth¹

¹*Department of Physics, Indian Institute of Science, Bangalore 560012, India*

²*Department of Physics, 500 W. University Ave, The University of Texas at El Paso, TX 79968, USA*

³*University of Missouri Research Reactor, University of Missouri, Columbia, MO 65211, USA*

⁴*Idaho National Laboratory, Idaho Falls, ID 83415, USA*

⁵*Central Department of Physics, Tribhuvan University, Kirtipur, 44613, Kathmandu, Nepal*

⁶*IFW Dresden, Helmholtzstr. 20, D-01069, Dresden, Germany*

(Dated: January 14, 2020)

The perovskite $\text{TbFe}_{0.5}\text{Cr}_{0.5}\text{O}_3$ shows two anomalies in the magnetic susceptibility at $T_N = 257$ K and $T_{\text{SR}} = 190$ K which are respectively, the antiferromagnetic and spin reorientation transition that occur in the Fe/Cr sublattice. Analysis of the magnetic susceptibility reveals signatures of Griffiths-like phase in this compound: the negative deviation from ideal Curie-Weiss law and in less-than-unity power-law susceptibility exponents. Neutron diffraction analysis confirms that, as the temperature is reduced from 350 K, a spin reorientation transition from Γ_2 (F_x, C_y, G_z) to Γ_4 (G_x, A_y, F_z) occurs at $T_N = 257$ K and subsequently, a second spin reorientation takes place from Γ_4 (G_x, A_y, F_z) to Γ_2 (F_x, C_y, G_z) at $T_{\text{SR}} = 190$ K. The Γ_2 (F_x, C_y, G_z) structure is stable until 7.7 K where an ordered moment of $7.74(1)\mu_B/\text{Fe}^{3+}(\text{Cr}^{3+})$ is obtained from neutron data refinement. In addition to the long-range order of the magnetic structure, indication of diffuse magnetic scattering at 7.7 K is evident, thereby lending support to the Griffiths-like phase observed in susceptibility. At 7.7 K, Tb develops a ferromagnetic component along the crystallographic a axis. Thermal conductivity, and spin-phonon coupling of $\text{TbFe}_{0.5}\text{Cr}_{0.5}\text{O}_3$ through Raman spectroscopy are studied in the present work. The magnetic anomalies at T_N and T_{SR} do not reflect in the thermal conductivity data of $\text{TbFe}_{0.5}\text{Cr}_{0.5}\text{O}_3$; however, it is noticeable that the application of 9 T magnetic field has no effect on the thermal conductivity. The T_N and T_{SR} are revealed in the temperature-dependence of full-width-at-half-maximum curves obtained from Raman intensities. An antiferromagnetic structure with ($\uparrow\downarrow\uparrow\downarrow$) arrangement of Fe/Cr spins is found in the ground state through first-principles energy calculations which supports the experimental magnetic structure at 7.7 K. The spin-resolved total and partial density of states are determined showing that $\text{TbFe}_{0.5}\text{Cr}_{0.5}\text{O}_3$ is insulating with a band gap of ~ 0.12 (2.4) eV within GGA (GGA+ U) functionals

I. INTRODUCTION

Rare earth orthoferrites and orthochromites with the general formula RMO_3 , where R = rare earth or yttrium and M = Fe or Cr, crystallize in the perovskite structure (usually $Pbnm$ space group) with orthorhombic distortion and an antiferromagnetic ground state [1]. Rare earth orthoferrites possess a complex spin structure and have drawn considerable attention due to their unique physical properties [1] and potential applications such as ultrafast magneto-optical recording [2], laser-induced thermal spin reorientation [3], precision excitation induced by terahertz pulses [4], inertia-driven spin switching [5], and magnetism-induced multiferroicity [6]. Most orthoferrites are G-type canted antiferromagnets with a weak ferromagnetic component due to Dzyaloshinskii-Moriya (DM) interaction and show temperature-induced spin reorientation (SR) from one magnetic symmetry to another. In $R\text{FeO}_3$, exchange interactions between $\text{Fe}^{3+}-\text{Fe}^{3+}$, $R^{3+}-\text{Fe}^{3+}$ and $R^{3+}-R^{3+}$ play an important role in determining complex magnetic structures. Isotropic $\text{Fe}^{3+}-\text{Fe}^{3+}$ exchange interac-

tion determines the magnetic structure of Fe^{3+} spins below the antiferromagnetic ordering temperature. Exchange field due to Fe^{3+} moment polarizes the R^{3+} spins of the R sublattice and the $\text{Fe}^{3+}-R^{3+}$ interaction, in turn, generates effective fields on Fe^{3+} spins which undergo spin reorientation transition and align perpendicular to the R^{3+} spins. The spin reorientation transition might be continuous or abrupt depending on the R element [7].

In TbFeO_3 , an unusual incommensurate magnetic phase was discovered [8] and it was shown that the exchange of spin waves between extended topological defects could result in novel magnetic phases which draws parallels with the Yukawa forces that mediate between protons and neutrons in a nucleus. The Fe^{3+} moments in TbFeO_3 exhibit $G_x A_y F_z$ ($Pb'n'm'$) spin configuration at room temperature [9–11] which is accompanied by a spin reorientation to $F_x C_y G_z$ ($Pbn'm'$). At 3 K, another spin reorientation occurs to revert to the $G_x A_y F_z$ ($Pb'n'm'$) structure. In recent years, a variety of interesting properties were achieved by substituting Fe ion by different transition metal ions [12, 13]. According to Goodenough-Kanamori rules [14], Cr^{3+} is a good choice to pair with Fe^{3+} to tune superior magnetic properties due to superexchange interaction between empty e_g orbital of Cr^{3+} and half filled e_g orbital of Fe^{3+} ions.

In TbCrO_3 , the exchange coupling between the nearest neighbour Cr^{3+} is predominantly antiferromagnetic and the

* Corresponding author email id: bhawana@iisc.ac.in

† Present address: Department of Physics, Bar-Ilan University Ramat-Gan, Israel

Cr^{3+} spins order spontaneously at $T_N = 167$ K [15]. Below this temperature, it exhibits weak ferromagnetism resulting from the canting of Cr^{3+} magnetic moments. In TbCrO_3 the Cr^{3+} spin structure is $G_z F_x$ below T_N and belongs to Γ_2 configuration which implies that the weak ferromagnet component of the Cr^{3+} moments orient along the a axis [16, 17].

Tb^{3+} spins order antiferromagnetically at 3.05 K [16] below which temperature the Tb^{3+} spin system exhibits an $A_x G_y$ structure. In the temperature range, $3.05 \text{ K} < T < T_N$ the Tb^{3+} spin system has $F_x C_y$ structure which belongs to Γ_4 representation and is coupled to the ordered Cr^{3+} spin system [16]. Spin reorientation, magnetization reversal and weak ferromagnetism is seen in compounds like $\text{TbFe}_{0.5}\text{Mn}_{0.5}\text{O}_3$ [18]. And reentrant spin reorientation transition has been seen in compounds like $\text{TbFe}_{0.75}\text{Mn}_{0.25}\text{O}_3$ [19] which undergo Γ_4 to Γ_1 transition and then, Γ_1 to Γ_4 transition. Recently, the magnetic structures and spin reorientation transitions of the mixed orthochromite–orthoferrite perovskites $\text{RFe}_{0.5}\text{Cr}_{0.5}\text{O}_3$, where $R = \text{Tb, Dy, Ho, Er}$ have been reported [20] using neutron diffraction.

In the present paper, we report a detailed study of magnetic phase transitions and magnetic structure of $\text{TbFe}_{0.5}\text{Cr}_{0.5}\text{O}_3$ through magnetization, neutron powder diffraction, Raman scattering and thermal conductivity studies in conjunction with density functional theory calculations. Our results support reentrant spin reorientation transition and a Griffiths phase–like features in the title compound. Our neutron scattering study also gives indication of diffuse magnetic component present below the T_N .

II. EXPERIMENTAL METHODS

Polycrystalline $\text{TbFe}_{0.5}\text{Cr}_{0.5}\text{O}_3$ was prepared by standard solid state reaction using high purity ($\geq 3\text{N}$) Tb_4O_7 , Fe_2O_3 and Cr_2O_3 in stoichiometric amounts. The starting materials were thoroughly mixed and sintered at 1200°C for 48 h with two times intermediate grinding. The phase purity of sintered sample was verified by taking powder X–ray diffractograms (PXRD) using Rigaku Smartlab X–ray diffractometer with Cu K_α radiation ($\lambda = 1.548 \text{ \AA}$). Oxidation states of Fe and Cr ions were determined using X–ray photoelectron spectroscopy (XPS) in a AXIS Ultra spectrometer and the data was analyzed using the CASA XPS spectroscopy software [21]. The chemical composition analysis of powder samples were performed using JEOL–JXA–8530F electron probe micro analyzer (EPMA) which yielded the Fe:Cr atomic ratio as 0.48:0.50 (Fe/Cr = 0.96). Temperature dependent DC magnetization measurements were performed on sintered pellets using a commercial magnetic property measurement system (MPMS, Quantum Design) in the temperature range of $5 \text{ K} \leq T \leq 400 \text{ K}$ at 100 Oe and 500 Oe in both zero–field cooled (ZFC) and field cooled (FC) protocols. Additionally, high temperature magnetic susceptibility was recorded up to 800 K in the high temperature VSM oven option provided with the physical property measurement system (PPMS). The thermal conductivity of a parallelepiped sample of $\text{TbFe}_{0.5}\text{Cr}_{0.5}\text{O}_3$

was measured in the temperature range 2 K–300 K in 0 T and 9 T magnetic field using a commercial physical property measurement system (PPMS).

To investigate nuclear and magnetic structure of $\text{TbFe}_{0.5}\text{Cr}_{0.5}\text{O}_3$, neutron powder diffraction experiments were performed at University of Missouri Research Reactor (MURR) using the neutron powder diffractometer, PSD. Neutron powder diffraction patterns of 2 g powder sample were collected at 350 K, 300 K, 215 K, 100 K and 7.7 K using neutrons of wavelength 1.485 \AA . The neutron diffraction data were analyzed using Fullprof suite of programs [22] employing the Rietveld method [23]. Magnetic representations belonging to the $Pbnm$ symmetry were determined using the software *SARAh* [24] and the corresponding magnetic structure was refined using Fullprof. Raman spectra was recorded from 110 K to 300 K temperature range in the backscattering geometry by using a HORIBA JOBIN–YVON spectrometer with 633 nm laser as an excitation source. Low temperature was maintained by closed cycle He–cryostat attached to spectrometer.

III. COMPUTATIONAL DETAILS

The electronic and magnetic structure calculations were performed by means of density–functional theory (DFT) approach using the full–potential linearized augmented plane wave plus local orbital method as implemented in the WIEN2k code [25]. The non–overlapping muffin–tin sphere radii (R_{MT}) of 2.35, 2.0, 1.96, and 1.72 Bohr were used for Tb, Fe, Cr, and O respectively. The linear tetrahedron method with 500 k points was employed for the reciprocal–space integrations in the whole Brillouin zone (BZ) that corresponds to 216 k –points within the irreducible BZ. For the calculations, the standard generalized–gradient approximation (GGA) in the parameterization of Perdew, Burke, and Ernzerhof (PBE–96) was used [26]. In order to consider the strong correlation effects, GGA+ U functional with double–counting corrections according to Anisimov *et al.* [27] was used. The chosen values of U were 6 eV for Tb– $4f$, 5 eV for Fe– $3d$, and 3 eV for Cr– $3d$ states, which are comparable to the values found in literature [28–33]. Calculations were performed using the lattice parameters obtained from neutron diffraction data at 7.7 K (see Table I). The energy and charge convergence was set to 10^{-6} Ry and 10^{-4} of an electron, respectively, for self–consistent calculations. To obtain the magnetic ground states, we have considered five magnetic configurations by computing their total energies. They are ferromagnetic (FM– $\uparrow\uparrow\uparrow$), two antiferromagnetic (AFM1– $\uparrow\downarrow\downarrow$ and AFM2– $\uparrow\downarrow\uparrow$) and two ferrimagnetic (FIM1– $\uparrow\uparrow\downarrow$ and FIM2– $\uparrow\uparrow\downarrow$). Here, the spin arrangements for two inequivalent atoms each of Fe and Cr atoms are arranged as Fe1, Fe2, Cr1 and Cr2, respectively.

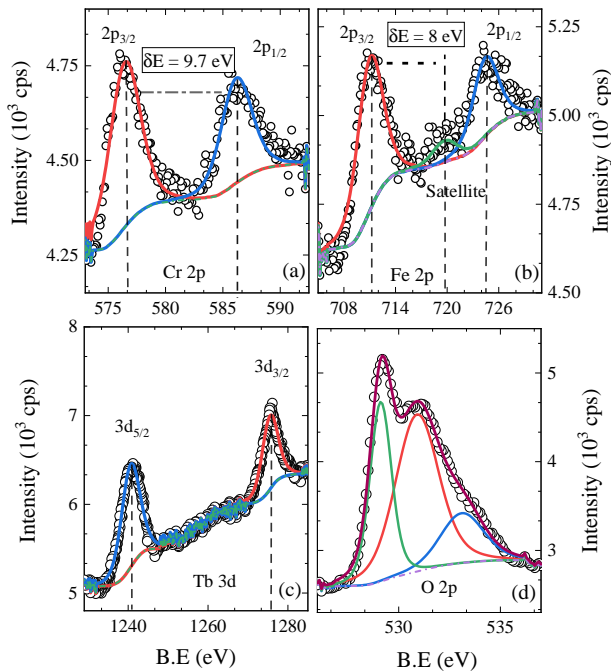


FIG. 1. X-ray photoelectron spectra of (a) Cr 2*p*, (b) Fe 2*p*, (c) Tb 3*d* and (d) O 2*p* are shown in open circles. Solid lines are fitted peaks, deconvoluted components and background, respectively, in each graph. Oxidation state of 3+ is inferred for Fe, Cr and Tb from this data.

IV. RESULTS AND DISCUSSION

A. X-ray photoelectron spectroscopy

Core level X-ray photoelectron spectroscopy measurements at room temperature using Al K_{α} X-ray source was performed to determine the valence states of cations in $\text{TbFe}_{0.5}\text{Cr}_{0.5}\text{O}_3$. Figure 1 shows the experimental intensities along with the peak fit obtained using the CASA XPS software. The core level binding energy was calibrated with carbon (B.E. = 284.8 eV). The Cr 2*p*_{3/2} peak at 576.5 eV is close to the binding energy of Cr_2O_3 (576 eV) [34]. However, in oxides, 2*p*_{3/2} peak of Fe^{2+} and Fe^{3+} appear around the binding energy values of 710.3 eV and 711.4 eV, respectively [35]. In $\text{TbFe}_{0.5}\text{Cr}_{0.5}\text{O}_3$, the peak at 711 eV is close to the binding energy value of Fe^{3+} . Additionally, a satellite peak at 8 eV above the Fe 2*p*_{3/2} confirms Fe^{3+} state (Fe^{2+} gives a satellite peak at 6 eV above the main Fe 2*p*_{3/2} peak). The XPS spectrum of Tb 3*d*_{5/2} yields a peak at 1240.8 eV which is very close to that of Tb_2O_3 peak (1241.2 eV) [36]. Our XPS results thus indicate 3+ oxidation state in Tb, Fe and Cr.

B. Magnetic properties: Spin reorientation and Griffiths-like phase

Figure 2 (a) shows the temperature dependent magnetization, $M(T)$, of $\text{TbFe}_{0.5}\text{Cr}_{0.5}\text{O}_3$ under ZFC and FC protocol at 100 Oe and 500 Oe external magnetic field.

Two anomalies are seen in the $M(T)$ curve at ≈ 257 K and at 190 K. A bifurcation of the ZFC and FC curves is seen below ≈ 15 K. With the application of 500 Oe, the bifurcation vanishes (see the inset of Figure 2(a)). The magnetic phase transition temperatures of $\text{TbFe}_{0.5}\text{Cr}_{0.5}\text{O}_3$ are determined by plotting dM/dT vs T as shown in top inset of Figure 2 (b). $T_{\text{SR}} = 190$ K and $T_N = 257$ K are identified in this manner. The temperature dependent inverse magnetic susceptibility, $\chi^{-1}(T)$, of $\text{TbFe}_{0.5}\text{Cr}_{0.5}\text{O}_3$ at 500 Oe is plotted in the main panel of Figure 2 (b) up to 800 K along with a curve fit using the Curie-Weiss (CW) law (dashed line), $\chi^{-1} = (T - \theta)/C$, where, $C = N_A \mu_{\text{eff}}^2 / 3k_B$ is the Curie constant, N_A is the Avogadro's number, μ_{eff} is the effective magnetic moment, k_B is the Boltzmann constant and θ is the Curie-Weiss temperature [37]. The Curie Weiss analysis yields an effective magnetic moment of $\mu_{\text{eff}} = 10.3(2) \mu_B$. Assuming 3+ oxidation state for Tb, Fe and Cr, as determined from the XPS analysis, the theoretically calculated magnetic moment, μ_{theory} in the paramagnetic region using the relation, $\mu_{\text{theory}} = \sqrt{\mu_{\text{Tb}}^2(\text{Tb}^{3+}) + 0.5 \times \mu_{\text{Cr}}^2(\text{Cr}^{3+}) + 0.5 \times \mu_{\text{Fe}}^2(\text{Fe}^{3+})}$ and considering high spin state of Tb^{3+} ($\mu_{\text{Tb}} = 9.7 \mu_B$), Fe^{3+} ($\mu_{\text{Fe}} = 5.9 \mu_B$) and Cr^{3+} ($\mu_{\text{Cr}} = 3.9 \mu_B$) is $10.9 \mu_B$.

A downward deviation of inverse magnetic susceptibility values from the ideal Curie-Weiss law is a signature of Griffith's phase (GP) [38–40]. The characteristic temperature at which the inverse susceptibility deviates from the CW behavior is known as the Griffiths temperature, T_G . It is clear from the main panel of Figure 2 (b) that the inverse susceptibility deviates from CW law above T_N at $T_G \approx 320$ K. The downturn softens with increase in applied magnetic field as shown in the lower inset of Figure 2 (b), this is a signature of the presence of Griffiths-like phase in the compound.

Figure 2 (c) shows the magnetization isotherms of $\text{TbFe}_{0.5}\text{Cr}_{0.5}\text{O}_3$ at 100 K, 220 K, 250 K, 300 K and 340 K measured upto ± 9 T which do not reveal strong ferromagnetic features. However, at 100 K, an opening of the magnetic hysteresis loop is observed at low applied field values (upper left inset of Figure 2 (c)). A magnified view of the isotherm at 340 K ($> T_N$) shown in lower inset of Figure 2 (c) reveals weak hysteresis indicating the presence of short range magnetism above T_N . In section IV C we present experimental evidences of spin fluctuation above T_N in $\text{TbFe}_{0.5}\text{Cr}_{0.5}\text{O}_3$.

We noted earlier that the downturn softening of the downturn in $\chi^{-1}(T)$ with an increase in applied field, supports GP scenario [41–43]. The suppression of downturn in magnetic susceptibility at high magnetic fields is due to the rising paramagnetic background which masks the ferromagnetic signal. Griffiths phase consists of finite size ferromagnetic (FM) clusters in a paramagnetic matrix well above the transition temperature in which the spins are ferromagnetically correlated within those clusters. However, the magnetic system as a whole does not have long-range ordering in GP and thus no spontaneous magnetization will appear. In GP, the FM clusters will appear with variable sizes having local ferromagnetic ordering due to which magnetization becomes non-analytic; in the low-field region, the magnetic suscep-

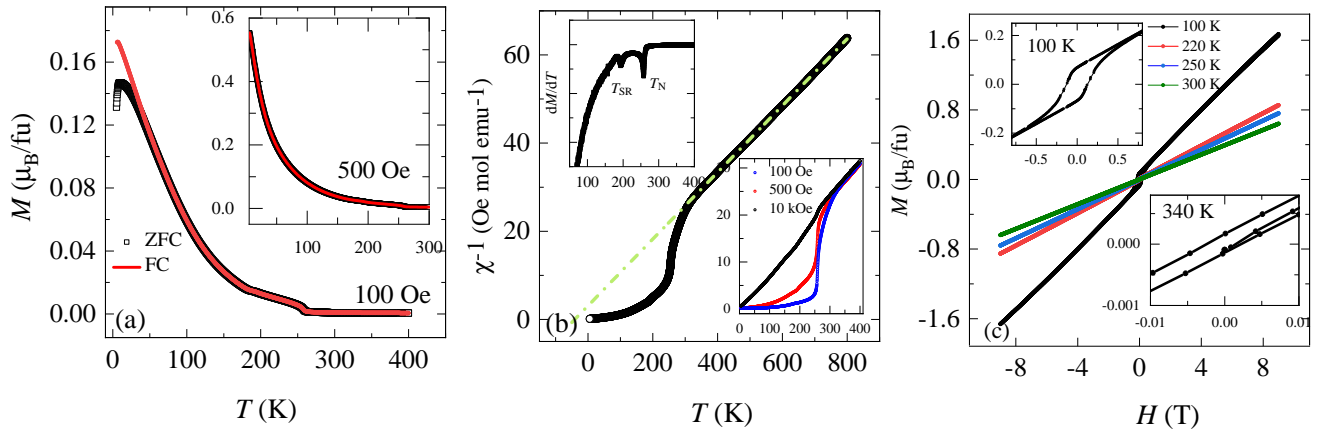


FIG. 2. (a) Magnetization as a function of temperature showing a bifurcation for ZFC and FC curves and the transitions at $T_N \approx 257$ K and $T_{SR} \approx 190$ K. The inset shows the magnetization at 500 Oe. (b) $\chi^{-1}(T)$ at 500 Oe along with Curie–Weiss fit (dashed line). The upper inset shows the derivative dM/dT where anomalies at T_N and T_{SR} are clear. The lower inset shows the inverse magnetic susceptibility at 100 Oe, 500 Oe and 10 kOe which shows that the negative curvature vanishes at higher fields. (c) The magnetization isotherms, $M(H)$, at 100 K, 220 K, 250 K and 300 K. A weak hysteresis that develops below the T_{SR} is shown in the upper inset ($T = 100$ K) and the lower inset shows a magnified view of a magnetization isotherm above the T_N ($T = 340$ K).

tibility will follow a power law behavior [41, 42, 44] given by, $\chi^{-1} \propto (T - T_c^R)^{1-\lambda}$, where T_c^R is the critical temperature of the FM clusters. Here susceptibility tend to deviate from CW law and λ ($0 \leq \lambda \leq 1$) is the exponent which signifies the deviation from CW behavior due to formation of magnetic clusters in the PM state above the transition temperature. A power law fit using the above-mentioned equation was administered on the magnetic susceptibility of $\text{TbFe}_{0.5}\text{Cr}_{0.5}\text{O}_3$ as $\log(\chi^{-1})$ versus $\log(T/T_c^R - 1)$ in both PM and GP regions as shown in Figure 3 (a). Since the value of λ is highly sensitive to T_c^R , we have proceeded to estimate the value of T_c^R accurately [42, 45]. The critical temperature of ferromagnetic clusters, T_c^R , is always greater than the transition temperature, so we first estimated the value of T_c^R in the purely paramagnetic region. This yields a value of 18 K which was later used in the curve-fitting for the Griffiths phase regime to obtain $\lambda = 0.99$. In the high temperature region, we obtained λ as 0.09 which signifies that the system is in paramagnetic phase, following the CW behavior. These values for λ are consistent with the GP model signifying a Griffiths singularity in $\text{TbFe}_{0.5}\text{Cr}_{0.5}\text{O}_3$.

Griffiths phase features are experimentally observed in strongly correlated systems like the layered iron pnictides [46] and in geometrically frustrated antiferromagnets [47]. In the case of the former, it is formed by randomly introduced localized magnetic impurities which form above the quantum critical point associated with the suppression of the stripe-antiferromagnetic spin density wave order. In the latter, the Griffiths phase was observed to be robust against the oxygen nonstoichiometry which influenced the antiferromagnetic ordering. Since the total magnetic susceptibility in the Griffiths phase region contains contributions from both paramagnetic as well as short-range correlated regions, the downturn observed in the inverse magnetic susceptibility from ideal CW law is not expected to be sharp in the case of antiferromagnetically correlated regions. In RFeO_3 , five

outer shell electrons of the Fe^{3+} ion are in half-filled e_g (σ -bond component) and t_{2g} (π -bond component) orbitals resulting in superexchange interactions that are antiferromagnetic. In the case of Cr^{3+} ions, superexchange interactions in the half-filled $t^3\text{-O-t}^3$ induce antiferromagnetism. Since Fe^{3+} and Cr^{3+} are randomly distributed in the lattice of $\text{TbFe}_{0.5}\text{Cr}_{0.5}\text{O}_3$, it results in stabilization of both ferromagnetic and antiferromagnetic couplings.

To confirm the GP-like scenario in antiferromagnetic $\text{TbFe}_{0.5}\text{Cr}_{0.5}\text{O}_3$, we employed thermoremanent magnetization protocol to measure magnetization (M_{TRM}), which has been used earlier to study spin glasses [48]. This protocol involves cooling the sample from well above the magnetic

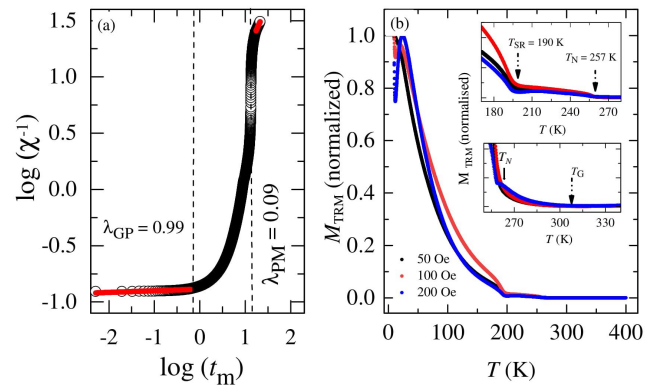


FIG. 3. (a) Shows the power law fits (red lines) to $\chi^{-1}(T)$ at 100 Oe; plotted in a log–log scale. The reduced-temperature is $t_m = (T/T_c^R - 1)$. (b) Thermoremanent magnetization, M_{TRM} , measured at 50 Oe, 100 Oe and 200 Oe cooling fields, showing the onset of spin reorientation transition T_{SR} and the antiferromagnetic T_N . The lower and upper insets show magnified regions near the T_N and T_{SR} , respectively.

transition temperature in the presence of a magnetic field. The field is then switched off below T_C , and the magnetization measured upon warming in zero field condition. The thermoremanent magnetization M_{TRM} will exhibit a sharp upturn at the transition temperature. In the present case of $\text{TbFe}_{0.5}\text{Cr}_{0.5}\text{O}_3$, this protocol was repeated for three different cooling fields, 50 Oe, 100 Oe and 200 Oe. The zero-field measurements performed here have the advantage that the contributions from the paramagnetic susceptibility are suppressed compared to an in-field measurement. Figure 3 (b) shows $M_{TRM}(T)$ measured at the different cooling fields. A clear signature of GP-like phase is seen in the form of an upturn in magnetization at temperature well above T_N . The T_G obtained from thermoremanent measurement is 315 K which is close to the value of 320 K estimated from magnetic susceptibility earlier.

C. Neutron diffraction: Reentrant spin reorientation and short-range spin correlations

The macroscopic magnetic measurements explicitly suggest the antiferromagnetic ordering at T_N , the possibility of a spin reorientation transition at T_{SR} and the presence of Griffiths-like phase in $\text{TbFe}_{0.5}\text{Cr}_{0.5}\text{O}_3$. We now proceed to investigate the magnetic structure of $\text{TbFe}_{0.5}\text{Cr}_{0.5}\text{O}_3$ in detail so as to understand the spin reorientation process and to ascertain the magnetic structures above and below the T_{SR} . For this purpose, neutron diffraction experiments were carried out on powder samples of $\text{TbFe}_{0.5}\text{Cr}_{0.5}\text{O}_3$ at various temperatures in the range of 7.7 K to 350 K.

The experimental neutron diffraction patterns at 350 K, 215 K, 100 K and 7.7 K are shown in Figures 4 (a-d) (red circles). Orthoferrites adopt orthorhombic structure as observed in a variety of $R\text{Fe}_{0.5}\text{Cr}_{0.5}\text{O}_3$ [49]. For $R = \text{Tb}, \text{Dy}, \text{Ho}$ and Er , the crystal structure belongs to a distorted perovskite type in the space group $Pbnm$ and ordered antiferromagnetically below 270 K in G_x configuration compatible with the Γ_4 representation. The above mentioned compounds exhibited a spin reorientation transition from G_x (Γ_4) to G_z (Γ_2). In present case of $\text{TbFe}_{0.5}\text{Cr}_{0.5}\text{O}_3$, refinement of the neutron diffraction data at 350 K was first performed using purely nuclear space groups, $P2_1/n$ and $Pbnm$. The perovskite structure in which cations order crystallographically may adopt a doubled unit cell with monoclinic $P2_1/n$ space group [50]. In $\text{TbFe}_{0.5}\text{Cr}_{0.5}\text{O}_3$, Rietveld analysis of the diffraction data at 350 K resulted in a reasonably good fit assuming $Pbnm$ space group, however, the intensity of the nuclear Bragg peak position (101) was not fully accounted for. Even at 350 K, appreciable contribution from magnetic scattering towards the total scattered intensity was observed.

In order to determine the magnetic structure, we scrutinized the symmetry-allowed magnetic structures for this class of compounds. It can be seen that for $R\text{FeO}_3$ compounds in $Pbnm$ space group, there exists eight irreducible representations Γ_1 through Γ_8 [1]. For the $4b$ Wyckoff position, the configurations Γ_5 to Γ_8 are incompatible with net moment on the Fe, and Γ_3 is not consistent with the observed strong antifer-

romagnetic coupling between nearest Fe neighbours. Hence only the remaining three representations are possible in orthoferrites [1]. The k -search utility in Fullprof was used for obtaining the propagation vector in the case of $\text{TbFe}_{0.5}\text{Cr}_{0.5}\text{O}_3$ and subsequently, SARA h was used to obtain the magnetic representations of the allowed magnetic structures. After testing the three different magnetic representations along with the nuclear phase in $Pbnm$, a better visual fit to the experimental data with reasonable agreement factors were obtained for Γ_2 , and was accepted as the solution of the magnetic structure at 350 K. The goodness-of-fit for the magnetic refinement, R_{mag} , for the three representations are as follows: $\Gamma_1 = 25.4$, $\Gamma_4 = 95.2$, $\Gamma_2 = 17.4$. Figure 4 (a) shows the neutron diffraction patterns at 350 K along with the refinement patterns using $Pbnm$ nuclear space group and the magnetic structure according to Γ_2 representation. The nuclear space group of

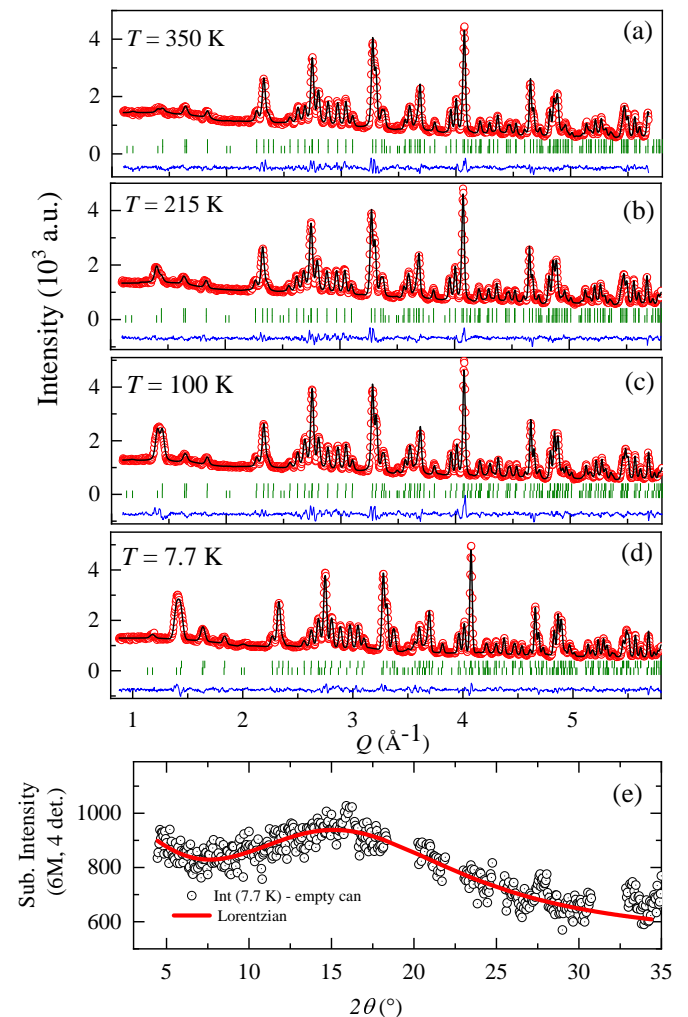


FIG. 4. (a-d) Rietveld refinement of the neutron powder diffraction patterns of $\text{TbFe}_{0.5}\text{Cr}_{0.5}\text{O}_3$ at 350 K, 215 K, 100 K, and 7.7 K using $Pbnm$ space group model. There is a weak magnetic contribution even at 350 K which is above the T_N , observed in magnetometry. (e) Diffuse scattering intensity at 7.7 K along with the curve fit (solid line) using a Lorentzian function.

TABLE I. Structural parameters and selected bond distances and bond angles of $\text{TbFe}_{0.5}\text{Cr}_{0.5}\text{O}_3$ at different temperatures obtained from neutron diffraction. The nuclear space group is $Pbnm$ where the atomic positions are Tb $4e$ (x, y, z), Cr/Fe $4b$ (0.5,0,0.5) and O $4e$ (x, y, z). Long (l) and short (s) bond lengths correspond to M -O(2) bonds in the ab plane. Medium (m) bond length corresponds to the out-of-plane M -O(1) apical bond.

	350 K	300 K	215 K	100 K	20 K	7.7 K
a (Å)	5.3111(4)	5.3125(6)	5.3100(6)	5.3121(0)	5.3140(5)	5.3124(2)
b (Å)	5.5548(1)	5.5560(5)	5.5517(5)	5.5442(0)	5.5403(4)	5.5391(3)
c (Å)	7.6117(8)	7.6111(0)	7.6039(1)	7.5963(3)	7.5929(1)	7.5917(3)
Fe(Cr)-O1 (m) (Å)	1.9885(5)	1.9902(4)	1.9886(0)	1.9866(5)	1.9858(6)	1.9850(6)
Fe(Cr)-O2 (l) (Å)	2.0106(0)	2.0115(4)	2.0120(3)	2.0083(8)	2.0076(0)	2.007(0)
Fe(Cr)-O2 (s) (Å)	1.9945(5)	1.9919(8)	1.9917(4)	1.9904(0)	1.9904(2)	1.9999(5)
Fe(Cr)-O1-Fe(Cr) $^\circ$	146.2(5)	145.9(0)	145.8(5)	145.8(5)	145.8(3)	145.9(2)
Fe(Cr)-O2-Fe(Cr) $^\circ$	147.2(4)	147.5(0)	147.2(3)	147.1(5)	147.5(1)	146.5(4)

$\text{TbFe}_{0.5}\text{Cr}_{0.5}\text{O}_3$ at all temperatures till 7.7 K was found to be $Pbnm$. The refined values of the lattice and bond parameters at different temperatures are given in Table I. Here, three different M -O bond lengths are listed. Long (l) and short (s) bond lengths correspond to M -O(2) bonds in the ab plane while the medium (m) bond length corresponds to the out of plane M -O(1) apical bond length which is almost parallel to the c axis.

As understood from the magnetization data presented in Figure 2 (a), a magnetic phase transition occurs in $\text{TbFe}_{0.5}\text{Cr}_{0.5}\text{O}_3$ at $T_N = 257$ K. Refinement of the diffraction pattern suggests that the nuclear structure is $Pbnm$ and the magnetic structure is Γ_4 ($Pb'n'm$) at 215 K. Thus, the magnetic structure changes from $\Gamma_2 \rightarrow \Gamma_4$ at T_N . The refined neutron diffraction pattern at 215 K is presented in Figure 4 (b). Interestingly, we observe a second spin reorientation transition back to the Γ_2 ($Pbn'm'$) structure at 100 K. This temperature is below T_{SR} (190 K) which is identified through the derivative of magnetization curve. The Γ_2 magnetic structure remains stable down to 7.7 K. In Figure 4 (e), the neutron diffraction intensity of $\text{TbFe}_{0.5}\text{Cr}_{0.5}\text{O}_3$ at 7.7 K is presented after subtracting the contribution of the empty vanadium can that was used as the sample holder. Preliminary evidence for diffuse magnetism is present in difference curves. This observation lends support to the short-range magnetic fluctuations with a close link to the features similar to those of Griffiths phase in the magnetization of $\text{TbFe}_{0.5}\text{Cr}_{0.5}\text{O}_3$. We attempted to analyze the diffuse intensity by fitting to the Lorentzian curve, which is shown as a red solid line in Figure 4 (e). The fit enabled us to extract a correlation length of approximately 9 Å. Elastisc and inelastic experiments are underway in single crystals of $\text{TbFe}_{0.5}\text{Cr}_{0.5}\text{O}_3$ to study the diffuse signatures.

Further, the rare earth magnetic atoms in $R\text{Fe}_{0.5}\text{Cr}_{0.5}\text{O}_3$ is reported to develop magnetic ordering at low temperature below 15 K [49]. Our data is in agreement to this observation. Our refinement at 7.7 K are consistent with the picture that the Tb^{3+} moments are magnetically ordered in $F_x C_y$ magnetic structure with a ferromagnetic component along the a axis. It is reported in a recent work [20] on $\text{TbFe}_{0.5}\text{Cr}_{0.5}\text{O}_3$ that only the C_y part remains whereas the ferromagnetic interactions disappear with the spin reorientation at 1.9 K. As

a result, diffuse magnetic scattering features emerge; this is well-captured in our work as can be seen in Figure 4 (e). The magnetic structures of the transition metal and rare earth moments as a function of temperature are shown in Figure 5.

D. Thermal conductivity and Raman spectroscopy

Figure 6 shows the thermal conductivity, $\kappa_t(T)$ of $\text{TbFe}_{0.5}\text{Cr}_{0.5}\text{O}_3$ measured in zero and in an applied magnetic field of 9 T. The overall magnitude and temperature dependence of the thermal conductivity suggest that the lattice thermal transport dominates in this material. As can be seen from the figure, there is no appreciable change in $\kappa_t(T)$ with the application of magnetic field. The relatively low value of $\kappa_t(T)$ might point to the presence of disorder in this material. In the context of the presence of the atomic disorder in UZr^2 and its impact to heat transport behavior, it is helpful to compare the measured thermal conductivity to the theoretically achievable minimum of the lattice contribution (fully disordered structure). In this model the $\kappa_{t(\text{min})}(T)$ dependence can be calculated by using Debye approximation and assuming that the transverse and longitudinal acoustic phonon modes are indistinguishable [51]. The results obtained for $\text{TbFe}_{0.5}\text{Cr}_{0.5}\text{O}_3$ using the Debye temperature, $\theta_D = 380$ K [52] and number of atoms per unit volume, $n = 4.7528 \text{ m}^{-3}$, are shown in Figure 6 by the blue solid line. The magnetic anomalies that occur at T_N and T_{SR} (seen in the derivative of magnetization) are absent in the derivative of $\kappa_t(T)$ (not shown here). In general, the behavior of $\kappa_t(T)$ of $\text{TbFe}_{0.5}\text{Cr}_{0.5}\text{O}_3$ is similar to the thermal conductivity variation in other $R\text{FeO}_3$ compounds like YFeO_3 , GdFeO_3 and DyFeO_3 [53]. However, in the work by Zhao *et al.* [53], single crystal samples of orthoferrites were studied in the milli-Kelvin temperature range and in external magnetic fields up to 14 T. In earlier studies of GdFeO_3 and DyFeO_3 , anomalies that occur in the vicinity of the magnetic transitions were reflected in the thermal conductivity response also [54, 55]. Significantly, low c axis thermal conductivity was observed in the case of YFeO_3 , GdFeO_3 and DyFeO_3 , considering that the present sample is a polycrystalline pellet, in comparison, we observed higher values

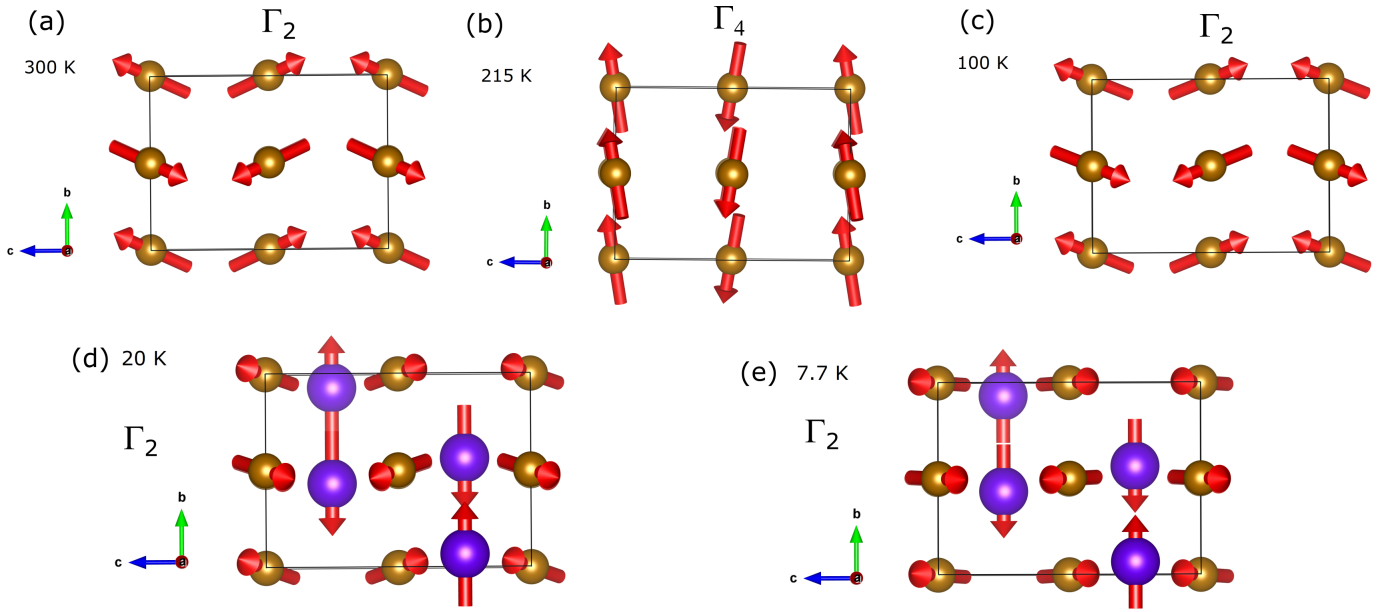


FIG. 5. (a, b, c) The magnetic structures of the Fe/Cr sublattice at 300 K (Γ_2), 215 K (Γ_4) and 100 K (Γ_2) respectively. The Γ_2 structure remains stable down to 7.7 K, which was the lowest probed temperature by neutrons in this study. (d and e) The magnetic structures of Tb^{3+} at 20 K and 7.7 K. The Fe/Cr atoms are represented as yellow spheres and Tb as blue

of thermal conductivity in $\text{TbFe}_{0.5}\text{Cr}_{0.5}\text{O}_3$. The total thermal conductivity could be compared to the T^3 boundary scattering limit of phonons [56]. In the inset of Figure 6, the temperature dependence of the T^3 form of $\kappa_t(T)$ is shown as a dashed line. The solid line is fitted to the $\kappa_t(T) \propto T^n$ expression where n is varied as a free parameter. Here, a value

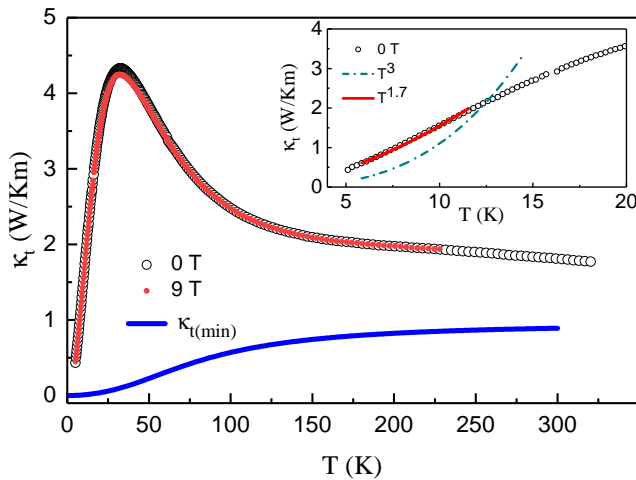


FIG. 6. Variation of thermal conductivity, $\kappa_t(T)$ of $\text{TbFe}_{0.5}\text{Cr}_{0.5}\text{O}_3$ as a function of temperature. As seen, there is no appreciable change in $\kappa_t(T)$ with the application of 9 T. The magnetic anomalies at T_N and T_{SR} seen in the derivative of magnetization are not observed in $\kappa_t(T)$ or in the derivative (not shown). The blue solid line represents the minimum thermal conductivity (see the text). In the inset, solid and the dashed lines represent $T^{1.7}$ and T^3 dependence of $\kappa_t(T)$ respectively.

of 1.7(3) was obtained for n . The $\kappa_t(T)$ curve of DyFeO_3 shows a weak curvature at low temperature (below 3 K) which is attributable to the magnonic contribution of Dy spin system [55]. Such a concave structure is not readily observed in the present case, however, the beginning of such a curvature could be discernible near 2 K.

Raman spectroscopy was carried out at different temperatures in order to understand the phonon behaviour across the magnetic transitions observed in $\text{TbFe}_{0.5}\text{Cr}_{0.5}\text{O}_3$. Raman spectra was recorded from 110 K to 300 K as shown in Figure 7 (top panel) with the most intense mode assignment matching with $R\text{FeO}_3$ [57] and $R\text{CrO}_3$ [58]. $\text{TbFe}_{0.5}\text{Cr}_{0.5}\text{O}_3$ is an orthorhombically distorted perovskite with $Pbnm$ space group symmetry. The irreducible representations corresponding to the phonon modes at the Brillouin zone center [59] can be defined as, $\Gamma = 7A_g + 7B_{1g} + 5B_{2g} + 5B_{3g} + 8A_u + 10B_{1u} + 8B_{2u} + 10B_{3u}$. Here, A_g , B_{1g} , B_{2g} , B_{3g} are the Raman active modes, B_{1u} , B_{2u} , B_{3u} are the infrared modes, and A_u is inactive mode. Among them, the modes which are above 300 cm^{-1} are related to the vibrations of oxygen, and the modes below 300 cm^{-1} are associated with the rare earth ions [60]. However, the Raman vibrational modes corresponding to an orthorhombic structure are A_g+B_{1g} and $2B_{2g}+2B_{3g}$, which are symmetric and anti-symmetric modes, respectively. In contrast, $A_g+2B_{1g}+B_{3g}$, $2A_g+2B_{2g}+B_{1g}+B_{3g}$, and $3A_g+B_{2g}+3B_{1g}+B_{2g}$ are associated with the bending modes, rotation and tilt mode of the octahedra, and for the rare earth vibrations, respectively [61]. Raman modes generally shifts to low frequency as the temperature increases accompanied by a monotonic increase in full-width-at-half-maximum (FWHM) [62]. This is mainly due to the expansion of lattice as thermal energy increases.

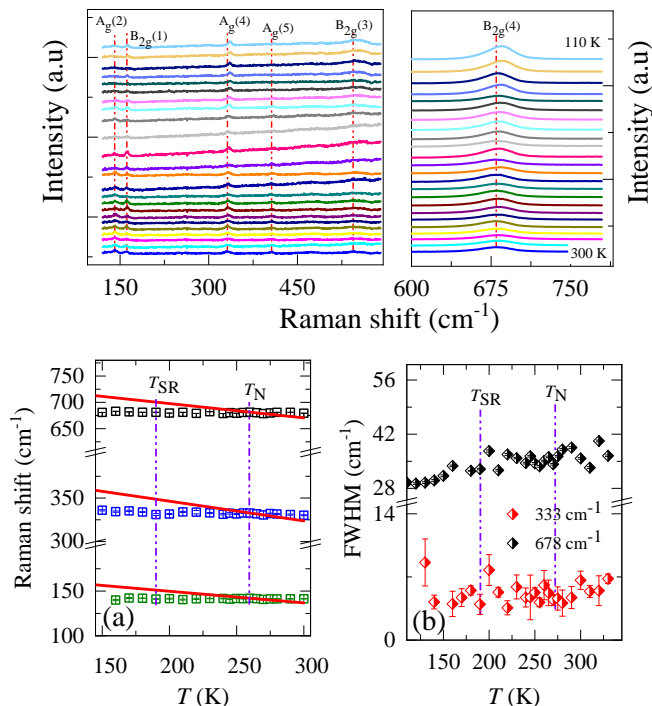


FIG. 7. Top panel: Raman spectrum of $\text{TbFe}_{0.5}\text{Cr}_{0.5}\text{O}_3$ at different temperatures along with the most intense phonon modes assigned. (a) Shows temperature dependence of phonon frequency obtained from the fit of the spectral profile with Lorentzian function. Red solid line shows anharmonic function fitting. (b) Shows temperature dependence of phonon linewidth. Vertical violet dashed line shows position of T_N and T_{SR} .

Absence of any extra peak indicates that the spectral symmetry remains same at all measured temperature thus confirming that the magnetic transitions are not associated with any structural phase transition. We analyzed well-resolved Raman modes in detail. These modes were fitted with Lorentzian function. The temperature variation of the phonon frequencies of modes $A_g(2)$ (141 cm^{-1}), $A_g(4)$ (333 cm^{-1}) and $B_{2g}(4)$ (678 cm^{-1}) along with the fit assuming the standard anharmonic dependence [63] of phonon modes are shown in Figure 7 (a).

The anharmonic dependence of the modes is given by, $\omega_{\text{anh}}(T) = \omega_0 - C(1 + (2/(e^{(\hbar\omega/k_B T)} - 1))))$ where ω_0 is temperature-independent part of linewidth, C is a constant determined from the fitting, $\hbar\omega$ is the phonon energy, and k_B is the Boltzmann constant. The sudden change in the phonon frequency near T_N and T_{SR} can be clearly seen in Figure 7 (a). A similar kind of anomaly in Raman modes near the magnetic transition was reported in $R\text{CrO}_3$ [58] compounds. Magnetostriction can also give rise to similar anomalous behaviour in phonon frequency by modifying unit cell volume [62]. But in that case, FWHM remains unchanged as it corresponds to phonon lifetime which is not affected by subtle change in lattice volume caused by magnetostriction. But, from Figure 7 (b), it can be seen that FWHM abruptly drops near the magnetic transitions. The anomalous change in the mode frequencies and linewidths near the magnetic transition establishes

the spin-phonon coupling in $\text{TbFe}_{0.5}\text{Cr}_{0.5}\text{O}_3$. A similar signature of spin-phonon coupling was reported in $R\text{CrO}_3$ [58] and $\text{DyFe}_{0.5}\text{Cr}_{0.5}\text{O}_3$ [64]. The possible coupling mechanism involved is the phonon modulation of superexchange integral below the magnetic ordering temperature [65].

E. Density functional theory calculations

From the total energy calculations for five different collinear magnetic configurations, AFM1 ($\uparrow\downarrow\downarrow$) is found to be most stable with the lowest energy. The AFM1 spin structure is found to be consistent with our experimental observation for the Γ_2 state at 7.7 K. Similarly, the first excited AFM2 configuration is consistent with the spin structure for the Γ_4 state at 300 K whose total energy is ~ 36 meV per formula unit higher compared to the AFM1 state of $\text{TbFe}_{0.5}\text{Cr}_{0.5}\text{O}_3$. The order of relative stability of the magnetic states are AFM1 > AFM2 > FIM2 > FIM1 > FM. This may be an indication of the competing ground state between AFM1 and AFM2 observed as a Griffiths phase transition from Γ_2 to Γ_4 and, subsequently, the reentrant to Γ_2 phase as seen in Figure 5. The magnetic anisotropy energy calculated is ~ 4.68 meV per formula unit of $\text{TbFe}_{0.5}\text{Cr}_{0.5}\text{O}_3$ with in-plane easy axes. In $\text{TbFe}_{0.5}\text{Cr}_{0.5}\text{O}_3$, the lanthanide Tb takes the charge state $3+$ with $4f^8$ configuration. Likewise, the transition element Fe nominally takes the charge state $3+$ with $3d^5$ and Cr with charge state $3+$ should take the $3d^3$ configurations, respectively. In the stable AFM1 state, the calculated spin moment at each site of Tb, Fe and Cr are $\pm 5.9\ \mu_B$, $\pm 3.65\ \mu_B$, and $\pm 2.36\ \mu_B$, respectively. Their respective orbital moments are $\pm 1.03\ \mu_B$, $\pm 0.05\ \mu_B$, and $\mp 0.034\ \mu_B$ respectively. With GGA+ U effects, the spin moment of Tb, Fe and Cr turns out to $\pm 5.97\ \mu_B$, $\pm 4.14\ \mu_B$, and $\pm 2.57\ \mu_B$ respectively. The total magnetic moment compensates to zero as Tb, Fe and Cr couples antiferromagnetically among each other as observed in Figure 5.

We now proceed to the electronic structure of $\text{TbFe}_{0.5}\text{Cr}_{0.5}\text{O}_3$ in AFM1 state within GGA and GGA+ U , respectively. The spin-resolved total and partial density of states (DOS) are shown in Figure 8. $\text{TbFe}_{0.5}\text{Cr}_{0.5}\text{O}_3$ is found to be insulating with a band gap of ~ 0.12 (2.4) eV within GGA (GGA+ U). The correlation effects ' U ' significantly changes the electronic behaviour. As seen in the partial DOS, the main contributions from Tb- $4f$ states that were observed around E_F are shifting away from each other. Those states that are fully occupied shift deep in the valence region while the un-occupied state moves far away in the conduction region. Similar features were observed also for Fe- $3d$ states around E_F . On the other hand, Cr- $3d$ states are contributing at and around E_F hybridizing strongly with the O- $2p$ orbitals (see partial DOS in Figure 8). This is mainly due to the hybridization between the $3d$ states of Cr and Fe with the O- $2p$ states. From the partial DOS contributions of Fe- $3d$, three t_{2g} and two e_g are fully occupied by five electrons in spin-up but in Cr- $3d$, three t_{2g} are fully occupied in spin up channel while e_g bands are empty.

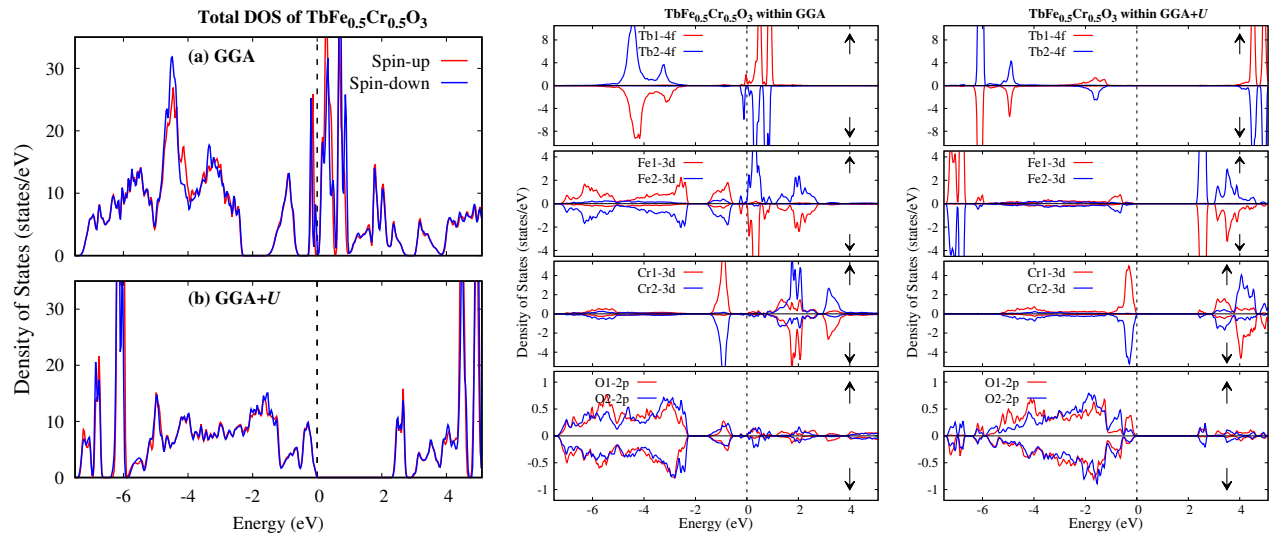


FIG. 8. Total and partial DOS of $\text{TbFe}_{0.5}\text{Cr}_{0.5}\text{O}_3$ in AFM1 configuration: Total DOS within GGA (top) and GGA+ U (bottom) (left) functionals; partial DOS contributions from Tb-4f, Fe-3d, Cr-3d and O-2p states, respectively within GGA (middle) and GGA+ U (right) functionals for the spin-up and spin-down channels.

V. CONCLUSIONS

We observe an antiferromagnetic transition T_N at 257 K and a spin reorientation transition T_{SR} at 190 K in the orthoferrite $\text{TbFe}_{0.5}\text{Cr}_{0.5}\text{O}_3$. Interestingly, a reentrant spin reorientation is seen in this compound, where the spins reorient again at 100 K. Through detailed neutron diffraction experiments and analysis we find that the spin structure changes from the Γ_2 representation at 350 K to Γ_4 at 215 K and then reverts to Γ_2 at 100 K. This structure remains stable until 7.7 K. A clear signature of Griffith phase is observed in the magnetization response of $\text{TbFe}_{0.5}\text{Cr}_{0.5}\text{O}_3$ and also short-range spin fluctuations that extend up to high temperature. The value of thermal conductivity is low in $\text{TbFe}_{0.5}\text{Cr}_{0.5}\text{O}_3$ which is not affected by the application of magnetic field of 9 T. The magnetic anomalies at T_N and T_{SR} are not directly seen in the thermal conductivity data, but the latter is dominated by the phonon contributions. Raman spectroscopic investigation reveals clear evidence of spin-phonon coupling in this compound.

VI. ACKNOWLEDGMENTS

The authors acknowledge Center for Nano Science and Engineering (CeNSE), Indian Institute of Science, Bengaluru. B.M. acknowledges financial support from University Grants commission (UGC), India for Senior research fellowship (SRF). H.S.N. acknowledges faculty start-up grant from UTEP and Rising Stars award. Work at INL was supported by DOE's Early Career Research Program. M.P.G. acknowledges the Higher Education Reform Project (HERP DLI-7B) of Tribhuvan University, Kirtipur, Nepal for the start-up grant, and Alexander von Humboldt Foundation, Germany for the partial support as return fellowship. S.R.B. thanks NAST, Nepal for the PhD fellowship, and IFW-Dresden for funding during research stay in Germany. M.P.G. and S.R.B. thanks Manuel Richter for the fruitful discussion and Ulrike Nitzsche for the technical assistance.

-
- [1] R. L. White, *Journal of Applied Physics* **40**, 1061 (1969), URL <https://doi.org/10.1063/1.1657530>.
- [2] A. V. Kimel, C. D. Stanciu, P. A. Usachev, R. V. Pisarev, V. N. Gridnev, A. Kirilyuk, and T. Rasing, *Physical Review B* **74**, 060403 (2006), URL <https://link.aps.org/doi/10.1103/PhysRevB.74.060403>.
- [3] A. V. Kimel, A. Kirilyuk, A. Tsvetkov, R. V. Pisarev, and T. Rasing, *Nature* **429**, 850 (2004), URL <http://dx.doi.org/10.1038/nature02659>.
- [4] J. Jiang, Z. Jin, G. Song, X. Lin, G. Ma, and S. Cao, *Applied Physics Letters* **103**, 062403 (2013), URL <https://doi.org/10.1063/1.4818135>.
- [5] A. V. Kimel, B. A. Ivanov, R. V. Pisarev, P. A. Usachev, A. Kirilyuk, and T. Rasing, *Nature Physics* **5**, 727 (2009), ISSN 1745-2481, URL <https://doi.org/10.1038/nphys1369>.
- [6] Y. Tokunaga, N. Furukawa, H. Sakai, Y. Taguchi, T.-h. Arima, and Y. Tokura, *Nature Materials* **8**, 558 (2009), URL <http://dx.doi.org/10.1038/nmat2469>.
- [7] T. Yamaguchi, *Journal of Physics and Chemistry of Solids* **35**, 479 (1974), URL <http://www.sciencedirect.com/science/article/pii/S002236977480003X>.
- [8] S. Artyukhin, M. Mostovoy, N. P. Jensen, D. Le, K. Prokes, V. G. de Paula, H. N. Bordallo, A. Maljuk, S. Landsgesell, H. Ryll, et al., *Nature Materials* **11**, 694 (2012), URL <http://>

- //dx.doi.org/10.1038/nmat3358.
- [9] Bourée, J.E. and Hammann, J., *Journal de Physique France* **36**, 391 (1975), URL <https://doi.org/10.1051/jphys:01975003605039100>.
- [10] E. Bertaut, J. Chappert, J. Mareschal, J. Rebouillat, and J. Sivadire, *Solid State Communications* **5**, 293 (1967), URL <http://www.sciencedirect.com/science/article/pii/0038109867902761>.
- [11] J. Tejada, X. X. Zhang, A. Roig, O. Nikolov, and E. Molins, *Europhysics Letters* **30**, 227 (1995), URL <http://stacks.iop.org/0295-5075/30/i=4/a=007>.
- [12] H. Taguchi, *Journal of Solid State Chemistry* **131**, 108 (1997), URL <http://www.sciencedirect.com/science/article/pii/S0022459697973552>.
- [13] A. Dahmani, M. Taibi, M. Nogues, J. Aride, E. Loudghiri, and A. Belayachi, *Materials Chemistry and Physics* **77**, 912 (2003), URL <http://www.sciencedirect.com/science/article/pii/S0254058402001888>.
- [14] J. B. Goodenough, *Physical Review* **100**, 564 (1955), URL <https://link.aps.org/doi/10.1103/PhysRev.100.564>.
- [15] J. D. Gordon, R. M. Hornreich, S. Shtrikman, and B. M. Wanklyn, *Phys. Rev. B* **13**, 3012 (1976), URL <https://link.aps.org/doi/10.1103/PhysRevB.13.3012>.
- [16] E. Bertaut, J. Mareschal, and G. D. Vries, *Journal of Physics and Chemistry of Solids* **28**, 2143 (1967), URL <http://www.sciencedirect.com/science/article/pii/0022369767902387>.
- [17] E. Bertaut, J. Mareschal, G. De Vries, R. Aleonard, R. Pauthenet, J. Rebouillat, and V. Zarubicka, *IEEE Transactions on Magnetics* **2**, 453 (1966), ISSN 1941-0069.
- [18] H. Nhalil, H. S. Nair, S. R., A. M. Strydom, and S. Elizabeth, *Journal of Applied Physics* **117**, 173904 (2015), URL <https://doi.org/10.1063/1.4919660>.
- [19] Y. Fang, Y. Yang, X. Liu, J. Kang, L. Hao, X. Chen, L. Xie, G. Sun, V. Chandragiri, C.-W. Wang, et al., *Scientific Reports* **6**, 33448 (2016), URL <http://dx.doi.org/10.1038/srep33448>.
- [20] J. P. Bolletta, F. Pomiro, R. D. Sánchez, V. Pomjakushin, G. Aurelio, A. Maignan, C. Martin, and R. E. Carbonio, *Physical Review B* **98**, 134417 (2018), URL <https://link.aps.org/doi/10.1103/PhysRevB.98.134417>.
- [21] N. Fairley, *Casa Software Ltd* **2005** (1999).
- [22] J. Rodriguez-Carvajal, *Physica B: Condensed Matter* **192**, 55 (1993), ISSN 0921-4526, URL <http://www.sciencedirect.com/science/article/pii/092145269390108I>.
- [23] H. M. Rietveld, *Journal of Applied Crystallography* **2**, 65 (1969), URL <https://doi.org/10.1107/S0021889869006558>.
- [24] A. Wills, *Physica B: Condensed Matter* **276-278**, 680 (2000), ISSN 0921-4526, URL <http://www.sciencedirect.com/science/article/pii/S0921452699017226>.
- [25] P. Blaha, K. Schwarz, G. K. Madsen, D. Kvasnicka, and J. Luitz, *An augmented plane wave+ local orbitals program for calculating crystal properties* (2001).
- [26] J. P. Perdew, K. Burke, and M. Ernzerhof, *Phys. Rev. Lett.* **77**, 3865 (1996), URL <https://link.aps.org/doi/10.1103/PhysRevLett.77.3865>.
- [27] V. I. Anisimov, F. Aryasetiawan, and A. I. Lichtenstein, *Journal of Physics: Condensed Matter* **9**, 767 (1997), URL <https://doi.org/10.1088%2F0953-8984%2F9%2F4%2F002>.
- [28] M. P. Ghimire, L.-H. Wu, and X. Hu, *Phys. Rev. B* **93**, 134421 (2016), URL <https://link.aps.org/doi/10.1103/PhysRevB.93.134421>.
- [29] M. P. Ghimire and X. Hu, *Materials Research Express* **3**, 106107 (2016), URL <https://doi.org/10.1088%2F2053-1591%2F3%2F10%2F106107>.
- [30] M. P. GHIMIRE, SANDEEP, and R. K. THAPA, *Modern Physics Letters B* **24**, 2187 (2010), URL <https://doi.org/10.1142/S0217984910024432>.
- [31] Y. Yuan, H. L. Feng, M. P. Ghimire, Y. Matsushita, Y. Tsujimoto, J. He, M. Tanaka, Y. Katsuya, and K. Yamaura, *Inorganic Chemistry* **54**, 3422 (2015), ISSN 0020-1669, URL <https://doi.org/10.1021/ic503086a>.
- [32] H. L. Feng, S. Calder, M. P. Ghimire, Y.-H. Yuan, Y. Shirako, Y. Tsujimoto, Y. Matsushita, Z. Hu, C.-Y. Kuo, L. H. Tjeng, et al., *Phys. Rev. B* **94**, 235158 (2016), URL <https://link.aps.org/doi/10.1103/PhysRevB.94.235158>.
- [33] H. L. Feng, M. P. Ghimire, Z. Hu, S.-C. Liao, S. Agrestini, J. Chen, Y. Yuan, Y. Matsushita, Y. Tsujimoto, Y. Katsuya, et al., *Phys. Rev. Materials* **3**, 124404 (2019), URL <https://link.aps.org/doi/10.1103/PhysRevMaterials.3.124404>.
- [34] G. C. Allen, M. T. Curtis, A. J. Hooper, and P. M. Tucker, *Journal of the Chemical Society, Dalton Transactions* pp. 1675–1683 (1973), URL <http://dx.doi.org/10.1039/DT9730001675>.
- [35] G. C. Allen, M. T. Curtis, A. J. Hooper, and P. M. Tucker, *Journal of the Chemical Society, Dalton Transactions* pp. 1525–1530 (1974), URL <http://dx.doi.org/10.1039/DT9740001525>.
- [36] B. D. Padalia, W. C. Lang, P. R. Norris, L. M. Watson, and D. J. Fabian, *Proceedings of the Royal Society of London. Series A, Mathematical and Physical Sciences* **354**, 269 (1977), URL <http://www.jstor.org/stable/79230>.
- [37] C. Kittel, *Introduction to Solid State Physics* (Wiley, New York, 1996).
- [38] R. B. Griffiths, *Phys. Rev. Lett.* **23**, 17 (1969), URL <https://link.aps.org/doi/10.1103/PhysRevLett.23.17>.
- [39] H. S. Nair, D. Swain, H. N., S. Adiga, C. Narayana, and S. Elizabeth, *Journal of Applied Physics* **110**, 123919 (2011), URL <https://doi.org/10.1063/1.3671674>.
- [40] T. Chakraborty, H. S. Nair, H. Nhalil, K. R. Kumar, A. M. Strydom, and S. Elizabeth, *Journal of Physics: Condensed Matter* **29**, 025804 (2016), URL <https://doi.org/10.1088%2F0953-8984%2F29%2F2%2F025804>.
- [41] A. K. Pramanik and A. Banerjee, *Phys. Rev. B* **81**, 024431 (2010), URL <https://link.aps.org/doi/10.1103/PhysRevB.81.024431>.
- [42] A. K. Pramanik and A. Banerjee, *Journal of Physics: Condensed Matter* **28**, 35LT02 (2016), URL <https://doi.org/10.1088%2F0953-8984%2F28%2F35%2F351t02>.
- [43] C. Magen, P. A. Algarabel, L. Morellon, J. P. Araújo, C. Ritter, M. R. Ibarra, A. M. Pereira, and J. B. Sousa, *Phys. Rev. Lett.* **96**, 167201 (2006), URL <https://link.aps.org/doi/10.1103/PhysRevLett.96.167201>.
- [44] R. B. Griffiths, *Phys. Rev. Lett.* **23**, 17 (1969), URL <https://link.aps.org/doi/10.1103/PhysRevLett.23.17>.
- [45] W. Jiang, X. Zhou, G. Williams, Y. Mukovskii, and R. Privezentsev, *Journal of Applied Physics* **107**, 09D701 (2010), URL <https://doi.org/10.1063/1.3335895>.

- [46] D. S. Inosov, G. Friemel, J. T. Park, A. C. Walters, Y. Texier, Y. Laplace, J. Bobroff, V. Hinkov, D. L. Sun, Y. Liu, et al., *Phys. Rev. B* **87**, 224425 (2013), URL <https://link.aps.org/doi/10.1103/PhysRevB.87.224425>.
- [47] J. Kumar, S. N. Panja, S. Dengre, and S. Nair, *Phys. Rev. B* **95**, 054401 (2017), URL <https://link.aps.org/doi/10.1103/PhysRevB.95.054401>.
- [48] R. Mathieu, P. Jönsson, D. N. H. Nam, and P. Nordblad, *Phys. Rev. B* **63**, 092401 (2001), URL <https://link.aps.org/doi/10.1103/PhysRevB.63.092401>.
- [49] J. P. Bolletta, F. Pomiro, R. D. Sánchez, V. Pomjakushin, G. Aurelio, A. Maignan, C. Martin, and R. E. Carbonio, *Phys. Rev. B* **98**, 134417 (2018), URL <https://link.aps.org/doi/10.1103/PhysRevB.98.134417>.
- [50] M. T. Anderson, K. B. Greenwood, G. A. Taylor, and K. R. Poepelmeier, *Progress in Solid State Chemistry* **22**, 197 (1993), ISSN 0079-6786, URL <http://www.sciencedirect.com/science/article/pii/007967869390004B>.
- [51] D. G. Cahill and R. Pohl, *Solid State Communications* **70**, 927 (1989), ISSN 0038-1098, URL <http://www.sciencedirect.com/science/article/pii/0038109889906303>.
- [52] M. Vagadia, S. Rayaprol, and A. Nigam, *Journal of Alloys and Compounds* **735**, 1031 (2018), ISSN 0925-8388, URL <http://www.sciencedirect.com/science/article/pii/S0925838817339440>.
- [53] J. Y. Zhao, Z. Y. Zhao, J. C. Wu, H. S. Xu, X. G. Liu, X. Zhao, and X. F. Sun, *AIP Advances* **7**, 055806 (2017), URL <https://doi.org/10.1063/1.4973293>.
- [54] Z. Y. Zhao, X. M. Wang, C. Fan, W. Tao, X. G. Liu, W. P. Ke, F. B. Zhang, X. Zhao, and X. F. Sun, *Phys. Rev. B* **83**, 014414 (2011), URL <https://link.aps.org/doi/10.1103/PhysRevB.83.014414>.
- [55] Z. Y. Zhao, X. Zhao, H. D. Zhou, F. B. Zhang, Q. J. Li, C. Fan, X. F. Sun, and X. G. Li, *Phys. Rev. B* **89**, 224405 (2014), URL <https://link.aps.org/doi/10.1103/PhysRevB.89.224405>.
- [56] R. Berman and P. G. Klemens, *Physics Today* **31**, 56 (1978).
- [57] M. C. Weber, M. Guennou, H. J. Zhao, J. Íñiguez, R. Vilarinho, A. Almeida, J. A. Moreira, and J. Kreisel, *Physical Review B* **94**, 214103 (2016), URL <https://link.aps.org/doi/10.1103/PhysRevB.94.214103>.
- [58] V. S. Bhadram, B. Rajeswaran, A. Sundaresan, and C. Narayana, *Europhysics Letters* **101**, 17008 (2013), URL <https://doi.org/10.1209%2F0295-5075%2F101%2F17008>.
- [59] S. Venugopalan, M. Dutta, A. K. Ramdas, and J. P. Remeika, *Physical Review B* **31**, 1490 (1985), URL <https://link.aps.org/doi/10.1103/PhysRevB.31.1490>.
- [60] M. K. Singh, H. M. Jang, H. C. Gupta, and R. S. Katiyar, *Journal of Raman Spectroscopy* **39**, 842 (2008), URL <https://onlinelibrary.wiley.com/doi/abs/10.1002/jrs.1923>.
- [61] M. N. Iliev, M. V. Abrashev, H.-G. Lee, V. N. Popov, Y. Y. Sun, C. Thomsen, R. L. Meng, and C. W. Chu, *Physical Review B* **57**, 2872 (1998), URL <https://link.aps.org/doi/10.1103/PhysRevB.57.2872>.
- [62] A. Nonato, B. S. Araujo, A. P. Ayala, A. P. Maciel, S. Yanez-Vilar, M. Sanchez-Andujar, M. A. Senaris-Rodriguez, and C. W. A. Paschoal, *Applied Physics Letters* **105**, 222902 (2014), URL <https://doi.org/10.1063/1.4902234>.
- [63] M. Balkanski, R. F. Wallis, and E. Haro, *Physical Review B* **28**, 1928 (1983), URL <https://link.aps.org/doi/10.1103/PhysRevB.28.1928>.
- [64] L. H. Yin, J. Yang, R. R. Zhang, J. M. Dai, W. H. Song, and Y. P. Sun, *Applied Physics Letters* **104**, 032904 (2014), URL <https://doi.org/10.1063/1.4862665>.
- [65] E. Granado, A. García, J. A. Sanjurjo, C. Rettori, I. Torriani, F. Prado, R. D. Sánchez, A. Caneiro, and S. B. Oseroff, *Physical Review B* **60**, 11879 (1999), URL <https://link.aps.org/doi/10.1103/PhysRevB.60.11879>.